

Overcoming Intrinsic Multidrug Resistance in Melanoma by Blocking the Mitochondrial Respiratory Chain of Slow-Cycling JARID1B^{high} Cells

Alexander Roesch,^{1,2,*} Adina Vultur,² Ivan Bogeski,³ Huan Wang,² Katharina M. Zimmermann,^{1,3} David Speicher,² Christina Körbel,⁴ Matthias W. Laschke,⁴ Phyllis A. Gimotty,⁷ Stephan E. Philipp,⁵ Elmar Krause,⁶ Sylvie Pätzold,⁸ Jessie Villanueva,² Clemens Krepler,² Mizuho Fukunaga-Kalabis,² Markus Hoth,³ Boris C. Bastian,⁹ Thomas Vogt,¹ and Meenhard Herlyn^{2,*}

¹Department of Dermatology, The Saarland University Hospital, D-66421 Homburg/Saar, Germany

²The Wistar Institute, 3601 Spruce Street, Philadelphia, PA 19104, USA

³Department of Biophysics

⁴Institute for Clinical and Experimental Surgery

⁵Department of Experimental and Clinical Pharmacology and Toxicology

⁶Department of Physiology

The Saarland University, D-66421 Homburg/Saar, Germany

⁷Department of Biostatistics and Epidemiology, University of Pennsylvania School of Medicine, 631 Blockley Hall, 423 Guardian Drive, Philadelphia, PA 19104, USA

⁸Department of Dermatology, Venereology, and Allergology, The University of Frankfurt, D-60590 Frankfurt, Germany

⁹Cardiovascular Research Institute, The University of California, San Francisco, 555 Mission Bay, Boulevard South, San Francisco, CA 94159, USA

*Correspondence: alexander.roesch@uks.eu (A.R.), herlynm@wistar.org (M.H.)

<http://dx.doi.org/10.1016/j.ccr.2013.05.003>

SUMMARY

Despite success with BRAFV600E inhibitors, therapeutic responses in patients with metastatic melanoma are short-lived because of the acquisition of drug resistance. We identified a mechanism of intrinsic multidrug resistance based on the survival of a tumor cell subpopulation. Treatment with various drugs, including cisplatin and vemurafenib, uniformly leads to enrichment of slow-cycling, long-term tumor-maintaining melanoma cells expressing the H3K4-demethylase JARID1B/KDM5B/PLU-1. Proteome-profiling revealed an upregulation in enzymes of mitochondrial oxidative-ATP-synthesis (oxidative phosphorylation) in this subpopulation. Inhibition of mitochondrial respiration blocked the emergence of the JARID1B^{high} subpopulation and sensitized melanoma cells to therapy, independent of their genotype. Our findings support a two-tiered approach combining anticancer agents that eliminate rapidly proliferating melanoma cells with inhibitors of the drug-resistant slow-cycling subpopulation.

INTRODUCTION

Malignant melanoma is a heterogeneous tumor of neuroectodermal origin that can be cured if excised at an early stage; however, once disseminated to distant organs, the median survival of patients drops below 9 months. All major cancer therapies

have failed to persistently increase melanoma patients' survival rates. This failure is attributed to different resistance mechanisms, including increased DNA repair and overexpression of antiapoptotic proteins, such as BCL-2, and drug efflux pumps, such as ABCB5 (Chen et al., 2009). Despite encouraging response rates seen with the BRAF inhibitor vemurafenib in

Significance

Metastatic melanoma is a heterogeneous tumor of neuroectodermal origin with a median survival less than 9 months. All chemotherapies, immunotherapies, and radiotherapies have failed to persistently increase survival. Despite the encouraging response rates following BRAFV600E targeting, relapses occur after a median duration of ~5 months, because melanoma cells acquire multiple resistance mechanisms. However, even among functionally and genetically heterogeneous tumors, common and intrinsic mechanisms exist that support the immediate survival of certain cells against the attack of cytotoxic agents. We have identified a subpopulation of slow-cycling, tumor-maintaining melanoma cells with intrinsic phenotypic resistance to various therapies, irrespective of their mode of action. Targeting the slow-cycling subpopulation could increase the efficacy of current treatment regimens and reduce relapses.

BRAFV600E-positive individuals, relapses occur after a median duration of ~5 months following initial tumor shrinkage (Sosman et al., 2012). Several groups have identified various mechanisms of acquired therapy resistance in BRAF-targeted melanomas. Surviving melanomas reactivate pivotal networks, such as the mitogen-activated protein kinase (MAPK) and phosphoinositide 3-kinase (PI3K) pathways (e.g., through activation of platelet-derived growth factor receptor β , cRAF-1 kinase, and insulin growth factor receptor 1 [Nazarian et al., 2010; Villanueva et al., 2010], dimerization of aberrantly spliced BRAF isoforms [Poulikakos et al., 2011], or by secondary genetic events, such as genomic amplification of *COT*, *NRAS* mutations, or the *MEK1C121S* mutation [Johannessen et al., 2010; Wagle et al., 2011]). However, even among functionally and genetically heterogeneous tumors, common and intrinsic survival mechanisms exist. Cytotoxic agents, including conventional chemotherapy, targeted therapy, or radiation, most effectively eliminate rapidly dividing cells (Blagosklonny, 2005). This concept is gaining prominence in the field of cancer research, with several studies reporting the enrichment of quiescent cancer stem cells after chemotherapy. For example, slow-cycling glioblastoma cells survive temozolomide treatment (Chen et al., 2012). Accordingly, if cell subpopulations can act as major drivers for tumor maintenance and mediate universal therapeutic resistance, approaches that target this phenotype could increase the efficacy of treatment regimens and reduce the risk of melanoma relapses.

We have recently demonstrated that, even within highly proliferative melanomas, there is a slow-cycling cell subpopulation that is identifiable by the expression of the histone 3 K4 demethylase JARID1B (Roesch et al., 2005, 2010). JARID1B (KDM5B/PLU-1/RBP2-H1) is a member of the highly conserved family of jumonji/ARID1 H3K4 demethylases, which are involved in tissue development, cancer, and stem cell biology (Christensen et al., 2007; Dey et al., 2008; Yamane et al., 2007). The JARID1B^{high} slow-cycling subpopulation is required for the continuous tumor growth of melanoma; however, it does not follow a unidirectional cancer stem cell hierarchy. The JARID1B^{high} phenotype is temporarily distinct, dynamic, and can be acquired depending on the microenvironmental context (Roesch et al., 2010). In this respect, another study indicates that other types of cancers, such as breast or lung cancer, also harbor populations of quiescent cells that are drug resistant and whose phenotypes can switch dynamically (Sharma et al., 2010). Interestingly, in the latter study, slow-cycling cells were characterized by the expression of the chromatin-remodeling factor JARID1A, a homolog of JARID1B.

Considering JARID1B's role in continuous tumor maintenance (Roesch et al., 2010), we asked (1) whether the subpopulation of JARID1B^{high} slow-cycling melanoma cells displays lower drug susceptibility compared to the bulk of tumor cells and (2) whether this resistant phenotype can be pharmacologically eradicated.

RESULTS

Cytotoxic Treatment of Melanoma Cells Results in the Enrichment of a Surviving JARID1B^{high} Slow-Cycling Subpopulation

To assess whether slow-cycling melanoma cells show differences in the therapeutic response compared to the rapidly prolif-

erating bulk, we treated melanoma cultures with various anticancer drugs. To discriminate between slowly and rapidly cycling subpopulations, we used a JARID1B- promoter-EGFP-reporter construct, as previously described (Roesch et al., 2010). This fluorescence-based model allows both the detection of slow-cycling melanoma cells based on their expression of JARID1B and monitoring of the dynamic nature of the JARID1B phenotype while cells are alive and interacting with their microenvironment. Prior *in vitro* and *in vivo* expression studies confirmed the correlation between the endogenous expression of JARID1B and the JARID1B promoter-induced expression of EGFP (J/EGFP) using an analytical threshold set to the maximum 5% of the fluorescence signal (Figure S1A available online; Roesch et al., 2010). Cells with an EGFP signal above this threshold show the highest endogenous JARID1B levels and, thus, can be reliably selected and analyzed. Two genetically different melanoma cell lines, WM3734 and 1205Lu, were stably transduced with this reporter construct and named WM3734^{JARID1Bprom-EGFP} and 1205Lu^{JARID1Bprom-EGFP}.

When the cell lines were treated with cisplatin at a highly toxic concentration (20 μ M) for 24, 48, and 72 hr, a gradual separation of the total population emerged into live, 7-aminoactinomycin (7AAD)⁻ and dead, 7AAD⁺ subpopulations (Figure 1A). With increasing incubation time, 7AAD⁻ cells were incrementally enriched for J/EGFP^{high} cells, whereas 7AAD⁺ cells were relatively J/EGFP^{low}. Control cells stably expressing a cytomegalovirus (CMV)-promoter-EGFP-reporter construct failed to show such a separation/enrichment pattern. While the total number of cells was constantly decreasing with rising cisplatin doses, the relative number of J/EGFP^{high} cells was significantly increasing in the drug-resistant population (Figures 1B and S1B). For example, up to 30.2% J/EGFP^{high} cells were seen following 20 μ M of cisplatin addition, compared to the 5% seen in vehicle controls. Immunoblotting confirmed an ~3-fold enrichment for endogenous JARID1B protein after densitometric normalization to glyceraldehyde 3-phosphate dehydrogenase (GAPDH) (Figure 1C). Vemurafenib also failed to eradicate all melanoma cells and enriched for J/EGFP^{high} cells, however, to a lesser extent than seen for cisplatin (Figure 1D). Interestingly, even when high concentrations of vemurafenib were applied, a distinct subpopulation of cells remained alive (7AAD⁻) and displayed an ~3-fold higher fluorescence intensity for J/EGFP (GMean = 25.55) than the population of vemurafenib-sensitive (7AAD⁺) cells (GMean = 8.54; Figure 1D). The surviving melanoma cells did not change in their mutational status of BRAF, as confirmed by DNA sequencing before and after treatment (data not shown). In a previous publication, we excluded the acquisition of secondary mutations for a large panel of diverse melanoma cell lines rendered resistant to BRAF inhibitors. We have tested 451Lu, Mel1617, WM983B, WM902B, and SKMel28 (parental and resistant pairs; several passages) for mutations in *BRAF*, *NRAS*, *TP53*, *PTEN*, *KIT*, *MEK1*, *MEK2*, *AKT1*, *CDKN2A*, and *CDK4* (Villanueva et al., 2010).

Interestingly, similar results were observed for other anti-cancer drugs, such as bortezomib and temozolomide (Figure 2A). We also note that a number of cells with relatively low J/EGFP expression can survive various drug treatments, indicating other potential operating mechanisms of phenotypic resistance. In contrast to its proposed effect on cancer stem

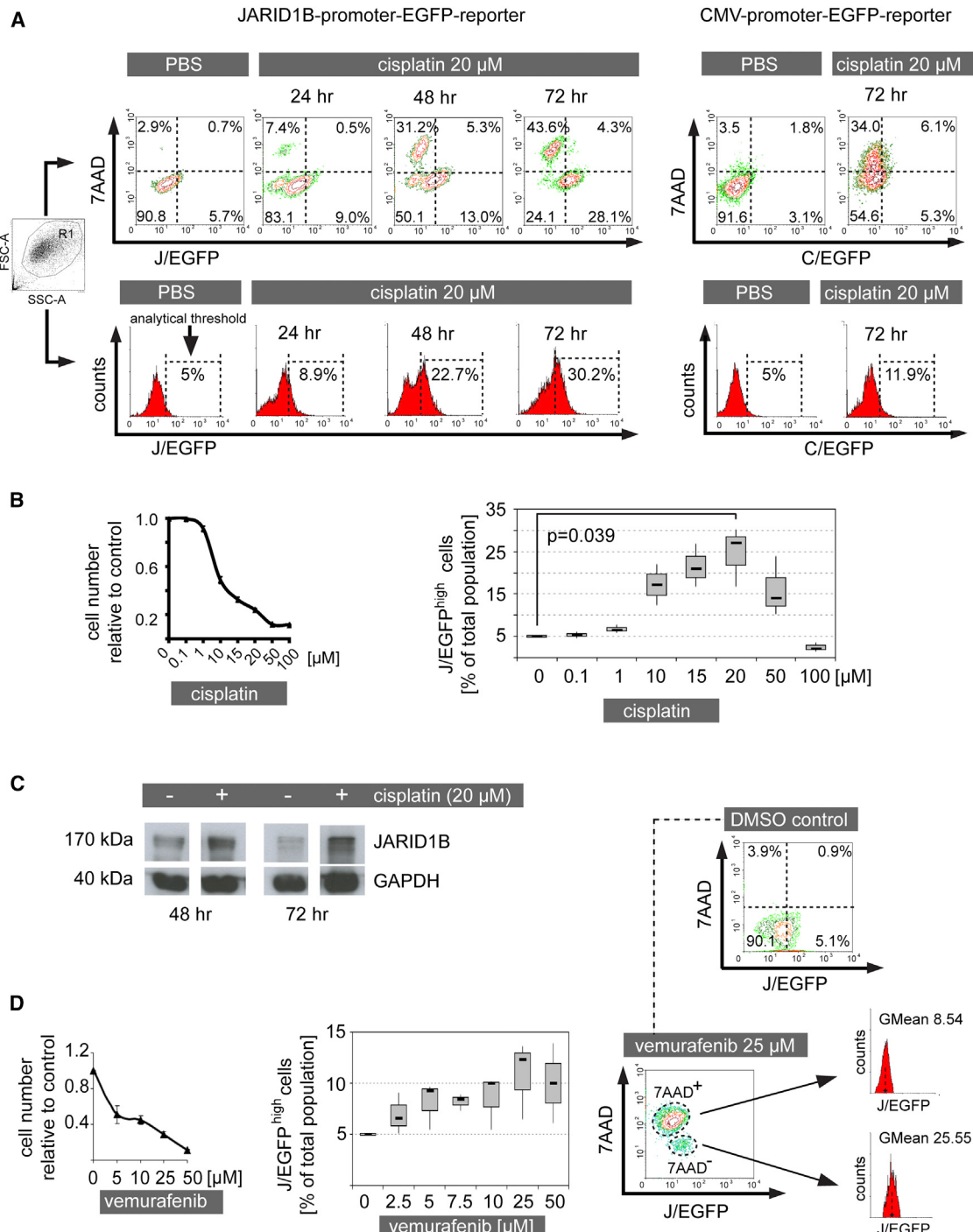


Figure 1. Cytotoxic Treatment Results in the Relative Enrichment of Therapy-Resistant JARID1B^{high} Melanoma Cells

(A) WM3734 melanoma cells were persistently treated with cisplatin and analyzed for J/EGFP expression by flow cytometry at the indicated time points (left). Dead cells were detected by 7AAD staining. Control cells were analyzed for C/EGFP expression (right). Depicted is one representative of at least three independently performed experiments.

(B) MTT cytotoxicity assay of WM3734 cells treated with increasing concentrations of cisplatin (left). Relative percentage of the J/EGFP^{high} subpopulation under escalating cisplatin treatment (right). Both panels show results from 72 hr of treatment.

(C) Immunoblot of JARID1B protein expression in pre- and postcisplatin-treated WM3734 cells at the indicated time points.

(D) Cytotoxicity assay and quantitation of the J/EGFP^{high} subpopulation after treatment of WM3734 cells for 72 hr with escalating vemurafenib concentrations (left and middle). Comparison of the J/EGFP expression levels of 7AAD⁺ and 7AAD⁻ cells (right). Error bars in the cytotoxicity assays represent SD. See also Figure S1.

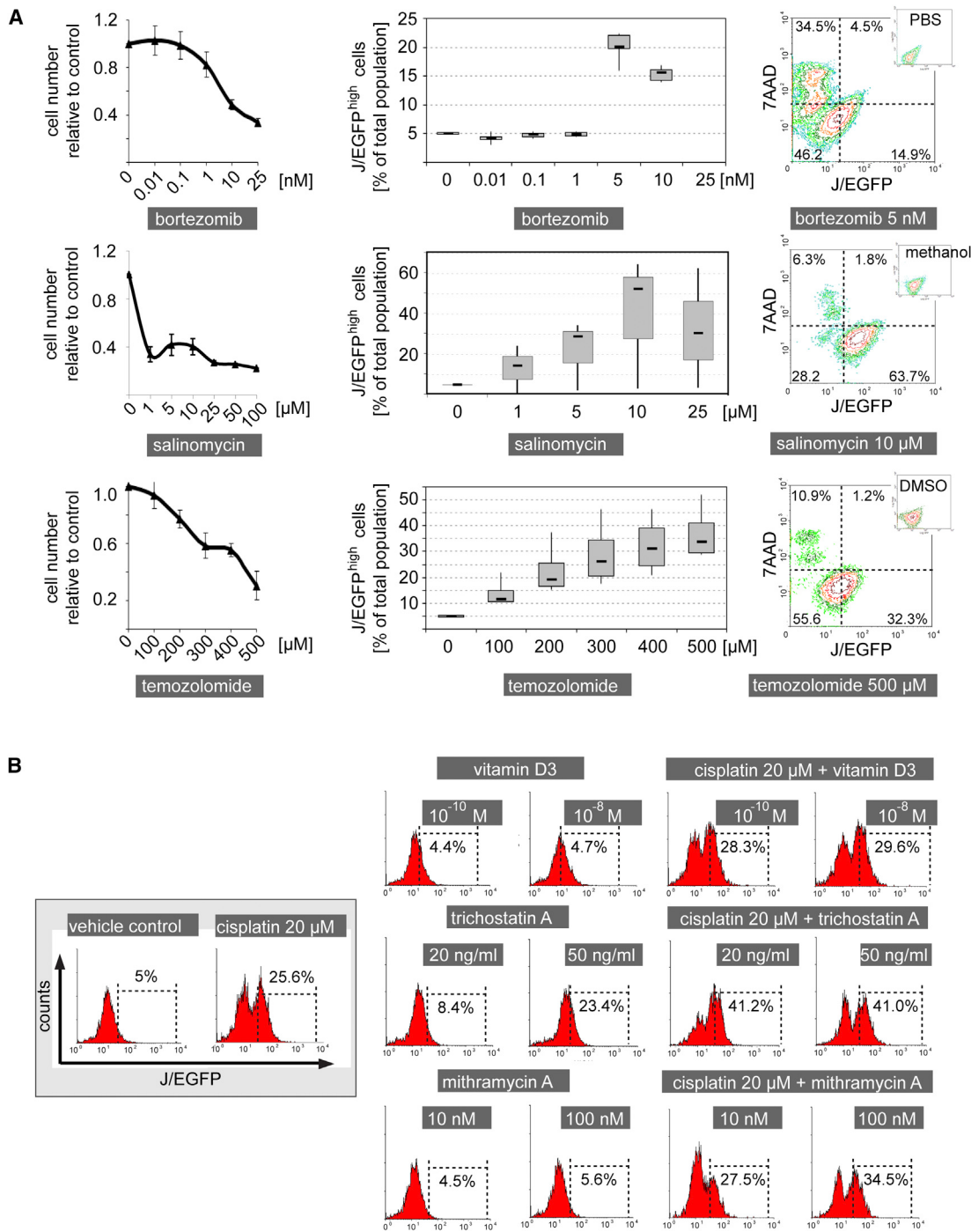


Figure 2. The JARID1B^{high} Subpopulation of Melanoma Cells Is Resistant to a Broad Panel of Anticancer Drugs

(A) Cytotoxicity assays of WM3734 cells after 72 hr of treatment with the indicated anticancer drugs (left). Flow cytometric determination of the relative percentage of the J/EGFP^{high} subpopulation under these treatments (middle). Typical examples for the corresponding drug-associated distribution of 7AAD and J/EGFP signals (right).

(B) Frequency of J/EGFP^{high} WM3734 cells as measured by flow cytometry after incubation with the indicated compounds over 72 hr. Error bars represent SD. See also Figure S2.

cells (Gupta et al., 2009), the potassium ionophore salinomycin also showed a strong enrichment of J/EGFP^{high} cells. To rule out an unspecific bias in our model, we tested vitamin D3 as

a compound with a different anticancer mechanism (prodifferentiation; Figure 2B). Here, no significant change in J/EGFP^{high} cells was seen. Next, we tested compounds that are expected

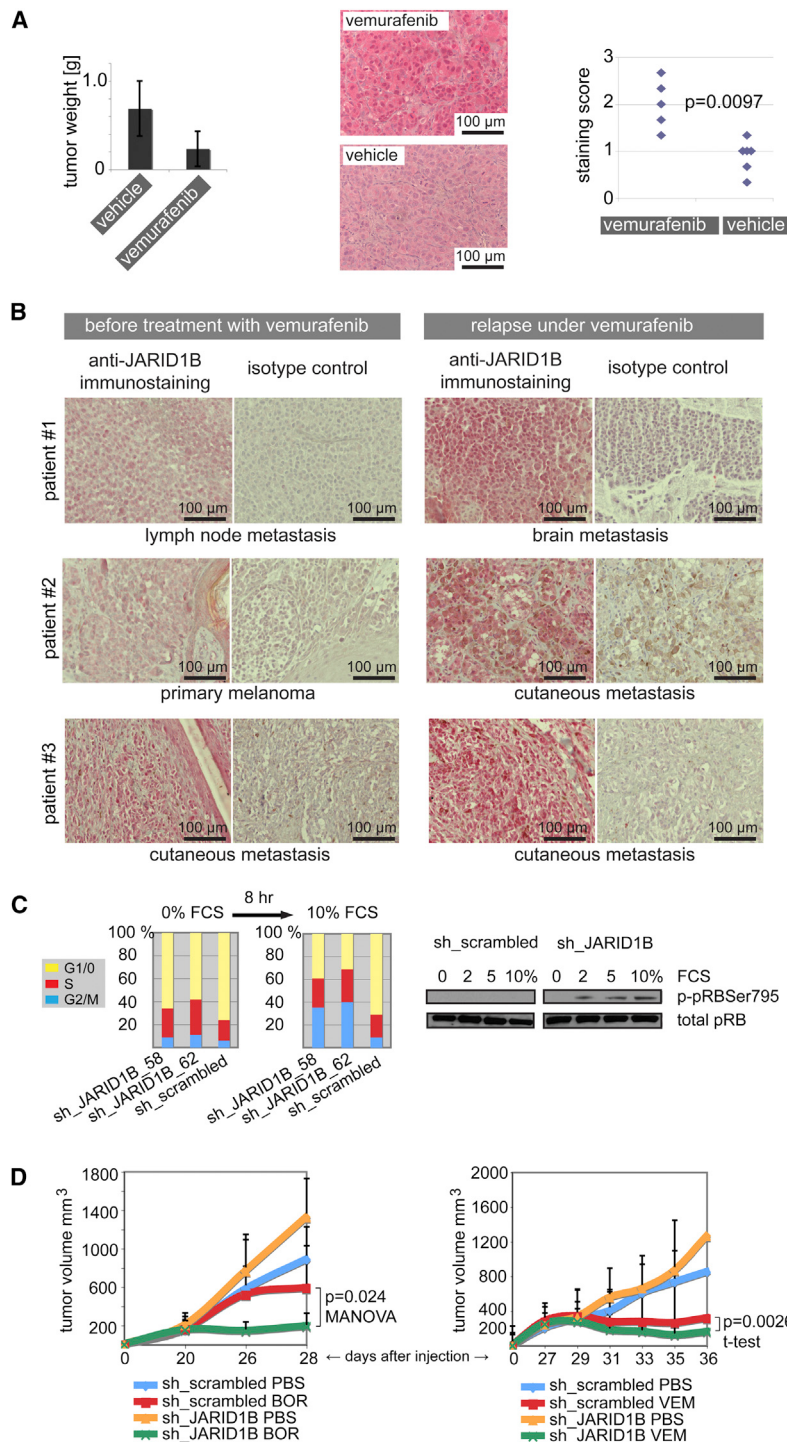


Figure 3. The JARID1B^{high} Subpopulation Is Enriched in Melanomas Resisting Therapy, and Knockdown of JARID1B Leads to Increased Drug Sensitivity

(A) NSG mice xenografted with WM3734 melanoma cells were treated with vemurafenib or vehicle ($n = 7$). Tumor weights were assessed after 11 days of treatment (left).

Tumor residues were immunostained for JARID1B expression (middle), and nuclear-staining signals of each tumor were scored at 40X magnification in three representative fields of vision (right, two-sided Wilcoxon two-sample test). (B) Immunostaining of JARID1B in matched pairs of melanoma samples before and relapse under vemurafenib treatment from three melanoma patients.

(C) Two different JARID1B knockdown clones (sh_JARID1B_58 and 62) of WM35 melanoma cells and the sh_scrambled control were starved for 4 days at 0% FCS and subsequently stimulated by 10% FCS for 8 hr. The bar graph shows one example of five independent experiments of propidium iodide-based cell cycle analysis (left). The immunoblot shows pRB phosphorylation (right).

(D) NSG mice were xenotransplanted with WM3734 melanoma cells stably knocked down for JARID1B (sh_JARID1B) or with control cells (sh_scrambled). Each mouse received 10^4 cells ($n = 8$). After tumors reached an average volume of $\sim 200 \text{ mm}^3$, mice were treated with bortezomib (left, BOR), vemurafenib (right, VEM), or vehicle (PBS). Tumor volumes were measured at the indicated time points. Error bars represent SD.

See also Figure S3.

2011), did not reduce the J/EGFP^{high} subpopulation in our model (Figure S2).

The in vivo relevance of our observations was confirmed in WM3734 cells xenografted to NOD/LtSscidIL2R γ ^{null} (NSG) mice and treated with vemurafenib (Figure 3A). While tumors decreased in size due to treatment, the number and staining intensity of resistant JARID1B^{high} cells significantly increased. Importantly, a clear increase in JARID1B-expressing cells could be observed in three out of four matched pairs of patients' melanomas that relapsed under vemurafenib (Figure 3B). Together, these data indicate a universal resistance of the slow-cycling JARID1B^{high} melanoma subpopulation against various anticancer agents.

Knockdown of JARID1B Leads to Increased In Vivo Sensitivity to Antimelanoma Treatment

Previous studies suggested that the abrogation of the slow-cycling phenotype by JARID1B-specific knockdown leads in vitro and in vivo to increased cell proliferation followed by melanoma exhaustion (Roesch et al., 2010). To quantify the shifts in cell-cycle progression, depending on the presence or absence of JARID1B, we performed cell-cycle experiments in WM35 melanoma cells stably knocked down for JARID1B (Figures 3C and S3). WM35 was chosen because changes in cell cycle of this low tumorigenic cell line could be better assessed compared to lines with high doubling

to diminish the slow-cycling phenotype, such as the histone deacetylase inhibitor trichostatin A (Sharma et al., 2010) or the Sp1 inhibitor mithramycin A (Sp1-binding sites within the JARID1B promoter are indicative of a possible regulatory potential); however, both compounds failed to reduce the J/EGFP^{high} subpopulation (Figure 2B). Similarly, leflunomide, which was suggested to interfere with developmental processes in melanocytes and melanoma growth (White et al.,

rate. Influences of cell densities and growth factors were considered. Cells were seeded at different densities and serum-starved at 0% fetal calf serum (FCS) for 4 days to synchronize the cell cycles. Under these conditions, knockdown of JARID1B led to an increase in S phase cells when compared to the control. Following stimulation with 2%, 5%, and 10% FCS over 4, 8, 16, and 24 hr, JARID1B knockdown cells shifted to G2/M. The most consistent changes in the cell cycle were seen after 8 hr of 10% FCS stimulation. Across five independently performed experiments, we saw an average decrease in G1 phase cells in JARID1B knocked down cells by ~20% (ranging from ~5% to 40%; the latter experiment is depicted in Figure 3C), while S phase cells increased by ~6% (~2%–12%), and G2/M phase cells by ~14% (~1%–31%). As predicted by previous studies showing JARID1B/retinoblastoma protein (pRB)-dependent cell cycle control (Roesch et al., 2006), JARID1B knockdown was accompanied by an increase in pRB phosphorylation at the JARID1B-specific phosphorylation site Ser795 (Figure 3C). Consequently, we asked if the inhibition of JARID1B could affect the therapeutic responsiveness of melanoma cells to anticancer drugs while releasing them from their slow-cycling phenotype. Indeed, stable knockdown of JARID1B in WM3734 melanoma cells xenografted to NSG mice led to increased cell proliferation accompanied by a significant sensitization to different treatments (Figure 3D). JARID1B knockdown plus bortezomib showed an additive effect, improving the moderate antimelanoma effect of bortezomib to an almost complete stasis of tumor growth. When we combined JARID1B knockdown with vemurafenib, which by itself dramatically prevents melanoma growth, we still observed a decrease in the average tumor volume below that of the treatment-starting volume. Because of the biological variability of tumor sizes, this effect was not significant in the multivariate analysis of variance (MANOVA), but an analysis of the change in the logarithm of volume per unit time by t test had significantly different rates. In sum, these results support the hypothesis that targeting the slow-cycling cell phenotype can sensitize melanoma to anticancer approaches, including chemotherapeutics and molecular-targeted drugs.

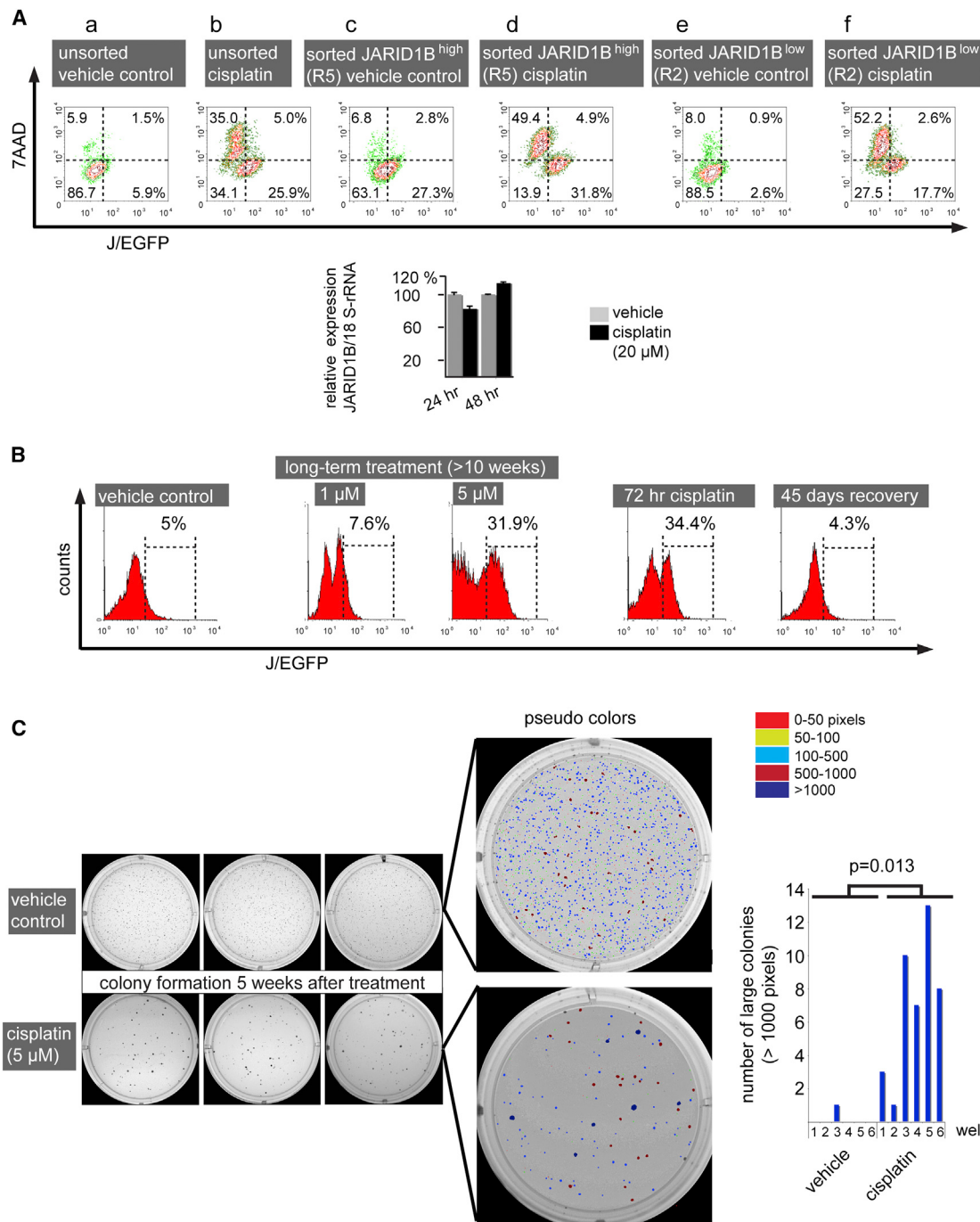
Dynamics of the Therapy-Resistant JARID1B^{high} Phenotype

According to our previous observations, the progeny of both J/EGFP^{high} and J/EGFP^{low} cells can dynamically interconvert into the opposing phenotype, indicating a flexible system that is dependent on the microenvironmental context (Roesch et al., 2010). Thus, we asked (1) if the newly developing progenies of initially sorted J/EGFP^{high} or J/EGFP^{low} cells show a differential drug response and (2) if the observed enrichment of J/EGFP^{high} cells after anticancer treatment results from selection of J/EGFP^{high} cells or induction of J/EGFP^{high} expression. In regular culture, spontaneous phenotype interconversion usually becomes visible within a few days after fluorescence-activated cell sorting (FACS) of the two populations. For example, 69.9% of FACS-sorted J/EGFP^{high} cells turned negative 72 hr after separation (Figure 4Ac, upper left plus lower left quadrant), while in total, 3.5% of the progeny of sorted J/EGFP^{low} cells became J/EGFP^{high} (Figure 4Ae). When sorted cells were treated with 20 μ M cisplatin for 72 hr, we saw no substantial enrichment for J/EGFP^{high} cells in the progeny of initially J/EGFP^{high} cells, indicating that no additional JARID1B-expression cells were induced (summarized upper and lower right quadrants; Figure 4Ac versus Figure 4Ad). Interestingly, most newly developed J/EGFP^{low} cells became 7AAD⁺ under cisplatin treatment (Figure 4Ac versus Figure 4Ad, upper and lower left quadrants). The apparent preference for JARID1B induction in the progeny of J/EGFP^{low} cells (Figure 4Ae versus Figure 4Af) was counteracted by an increased rate of cisplatin-induced cell death in cells derived from the J/EGFP^{low} population. Manual counts revealed a significantly lower number of surviving cells in the progeny of sorted J/EGFP^{low} cells compared to the progeny of J/EGFP^{high} cells ($p < 0.05$ for 5 μ M and 10 μ M cisplatin; data not shown). Together with the results from consecutive measurements of JARID1B messenger RNA (mRNA) under cisplatin treatment that did not show transcriptional upregulation (Figure 4A), we concluded that the major mechanism for the enrichment of J/EGFP^{high} cells following therapy is a selection of pre-existent JARID1B^{high} slow-cycling cells. However, to a lesser extent, JARID1B induction may also occur (e.g., shifting cells with intermediate JARID1B expression to higher levels).

When cells were long-term challenged with cisplatin, the J/EGFP^{high} subpopulation remained constantly elevated over several weeks in a dose-dependent manner. The cisplatin-induced elevation of J/EGFP^{high} cells was fully reversible following drug withdrawal (Figure 4B). In line with the concept of dynamic phenotype switching (Roesch et al., 2010), drug-resistant cells that are enriched for JARID1B can regain the original cell distribution and J/EGFP ratios after drug removal. Moreover, cisplatin-surviving JARID1B-enriched cells gave rise to fewer but significantly larger (i.e., rapidly growing) three-dimensional (3D) colonies in soft agar compared to untreated cells (Figure 4C). This observation is reminiscent of earlier clonogenicity and single-cell dilution assays showing that untreated FACS-isolated J/EGFP^{high} cells give rise to a rapidly proliferating progeny with elevated repopulation capacity when compared to JARID1B^{low} cells (Roesch et al., 2010).

Bioenergetic Metabolism Plays an Important Role in the Survival of Slow-Cycling Melanoma Cells

We next designed experiments to unravel druggable targets that are specifically activated in slow-cycling melanoma cells. Since global gene expression screening with complementary DNA microarrays did not provide significant hit candidates in FACS-sorted J/EGFP^{high} versus J/EGFP^{low} or JARID1B knockdown versus control cells (data not shown), we performed quantitative proteome profiling. Following our established protocols for isolation of slow-cycling melanoma cells (Roesch et al., 2010), we costained WM3734^{JARID1Bprom-EGFP} cells with the PKH26 dye and then FACS-isolated the label-retaining and J/EGFP^{high} subpopulation versus nonlabel-retaining J/EGFP^{low} cells after a period of 4 weeks of cell divisions. Prior to sorting, the cells were grown as melanospheres to attain a more stringent J/EGFP phenotype, as previously reported (Roesch et al., 2010). Tryptic digests of the cell lysates were analyzed by liquid chromatography-mass spectrometry/mass spectrometry. Label-free computational quantitation identified 423 proteins with significant expression changes between label-retaining J/EGFP^{high} cells and nonlabel-retaining J/EGFP^{low} cells with a p value < 0.001 . Unexpectedly, neither common cancer target

**Figure 4. Dynamics of the Therapy-Resistant JARID1B^{high} Phenotype**

(A) WM3734^{JARID1Bprom-EGFP} cells were FACS-sorted according to their J/EGFP expression, and the isolated subfractions were cultured as adherent monolayers overnight. After subsequent treatment for 72 hr, the frequencies of J/EGFP^{high} and J/EGFP^{low} cells were again quantified by flow cytometry. Dead cells were detected by 7AAD staining. JARID1B mRNA expression was quantified by quantitative PCR.

(B) Flow cytometric detection of J/EGFP^{high} WM3734 cells after prolonged incubation with different concentrations of cisplatin and after drug recovery.

(C) Colony-forming assay of WM3734 cells that underwent cytotoxic pulse treatment prior to seeding. Cells were treated for 72 hr with cisplatin or vehicle. Surviving cells were subsequently embedded into soft agar (2,000 cells/well). Colony sizes and numbers were digitally quantified and color-coded, with dark blue colonies representing large colonies above 1,000 pixels. Shown are results from two independent experiments, each performed in triplicate. Error bars represent SD.

nor drug resistance-related protein could be detected by this approach. Instead, we found a differential regulation of a number of mitochondrial proteins with particular functions in bioener-

getic metabolism (Table S1). Many of the upregulated proteins play a major role in cell respiratory electron transport (oxidative phosphorylation [OXPHOS]), such as nicotinamide adenine

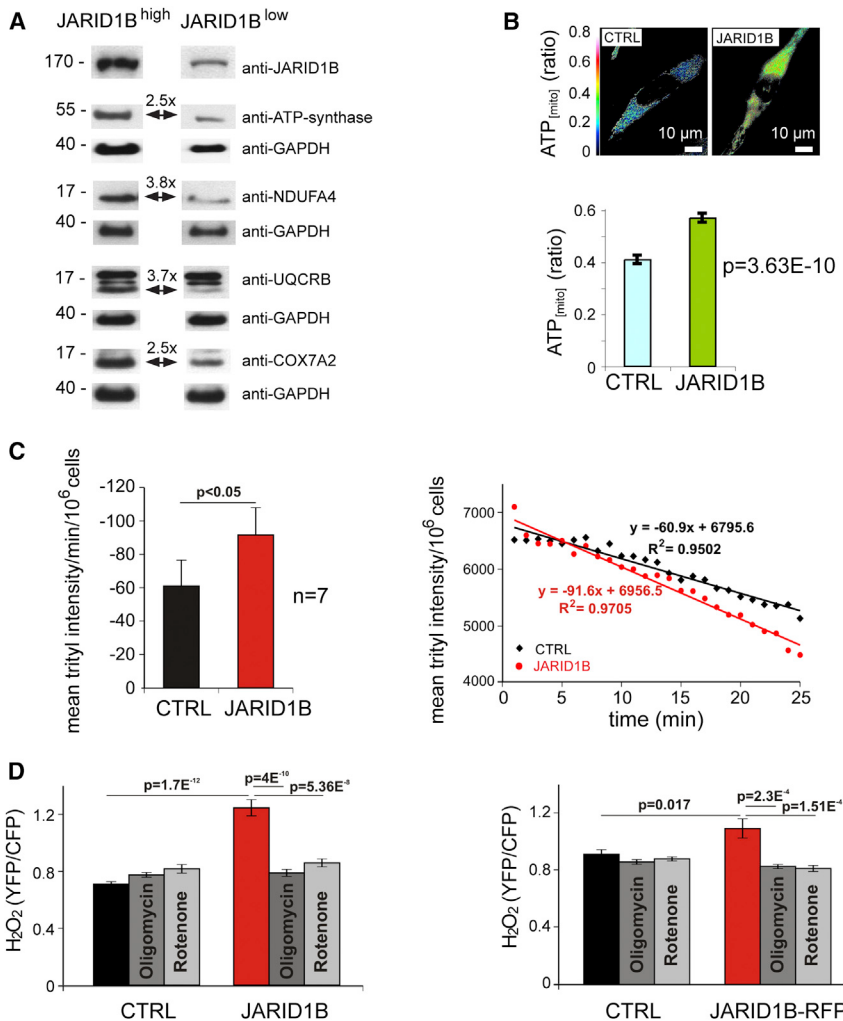


Figure 5. Elevated Mitochondrial Bioenergy Metabolism in the JARID1B^{high} Subpopulation

(A) Immunoblotting of mitochondrial respiratory enzymes in FACS-sorted J/EGFP^{high} and J/EGFP^{low} WM3734 cells. Fold changes were normalized to GAPDH.

(B) Relative mitochondrial ATP levels in control (CTRL) or JARID1B-transfected WM3734 cells were measured using the ATP sensor protein A_{TEAM} . Representative A_{TEAM} ratio images (top) and summarized A_{TEAM} ratio values in control ($n = 72$) and JARID1B-transfected ($n = 47$) cells (bottom).

(C) Mean oxygen consumption of control- (black) or JARID1B-transfected (red) WM3734 cells presented as decline of trityl radical intensity per minute per 10^6 cells (left). Mean oxygen concentration in presence of control or JARID1B-transfected WM3734 cells presented as trityl intensity per 10^6 cells. Each data point is an average of seven independent experiments.

(D) Relative H_2O_2 levels were measured in JARID1B-transfected WM3734 cells using the H_2O_2 sensor protein Hyper. Columns represent averaged Hyper ratio values of control- (black, $n = 71$) or JARID1B-transfected cells (red, $n = 48$). To test the role of mitochondria as source of H_2O_2 , cells were treated with $1 \mu M$ oligomycin (dark gray) or $1 \mu M$ rotenone (light gray). Numbers of cells averaged were: CTRL plus oligomycin ($n = 50$), CTRL plus rotenone ($n = 42$), JARID1B plus oligomycin ($n = 45$), and JARID1B plus rotenone ($n = 52$). In a confirmation experiment with WM3734 cells transfected with pCAGGS-JARID1B-IRES-RFP (right), positively transfected cells were selected for analysis based on the expression of red fluorescent protein (RFP). Error bars represent SEM.

See also Table S1.

dinucleotide (NADH) dehydrogenase (complex I of the mitochondrial electron transport chain), ubiquinol cytochrome c reductase (complex III), cytochrome c oxidase (complex IV), and ATP synthase. In contrast, glycolytic hexokinase I and II were down-regulated. Immunoblotting of lysates from J/EGFP-sorted cells confirmed upregulation of ATP synthase, NADH dehydrogenase, ubiquinol-cytochrome C reductase-binding protein, and cytochrome c oxidase in J/EGFP^{high} cells (Figure 5A). WM3734 cells transiently overexpressing JARID1B had a higher mitochondrial energy production compared to the mock control (Figure 5B). Accordingly, JARID1B-overexpressing WM3734 cells consumed ~50% more oxygen than control cells (Figure 5C). Treatment with different concentrations of oligomycin and rotenone severely reduced the oxygen consumption by up to 94%, indicating a major role for mitochondria in this process (data not shown). Because high mitochondrial electron transfer activity can lead to increase in superoxide and hydrogen peroxide (H_2O_2) production, we analyzed the H_2O_2 level. JARID1B-overexpressing cells generated 76% more H_2O_2 than control cells 60–72 hr after transfection (Figure 5D). The H_2O_2 increase was completely abolished by treatment with oligomycin or rotenone. These results suggest that redox signaling may play an important role

for JARID1B^{high} cells. Furthermore, high oxygen consumption can ultimately lead to hypoxic conditions, which is known to favor the JARID1B^{high} slow-cycling phenotype (Xia et al., 2009; Roesch et al., 2010).

Targeting the Mitochondrial Respiratory Chain Inhibits the JARID1B^{high} Subpopulation and Reveals Long-Term Effects against Melanoma Cells

Inhibition of the mitochondrial respiratory chain has been reported to exert tumor-suppressive effects in different types of cancers, including neuroectodermal glioblastoma cells (Hao et al., 2010). Since enzymes of almost all respiratory chain complexes were found differentially regulated in slow-cycling J/EGFP^{high} cells (Table S1), we explored representative inhibitory tool compounds, such as (1) the ATP-synthase inhibitors oligomycin and Bz-423, (2) the NADH dehydrogenase (complex I) inhibitors rotenone and phenformin, and (3) antimycin A, which inhibits the ubiquinol cytochrome c reductase in a series of preliminary cytotoxicity assays (data not shown). Here, ATP-synthase and complex I inhibitors revealed the most prominent results; thus, these were selected for subsequent studies. High concentrations of oligomycin were reported

to exert unspecific effects in eukaryotes, due to the uncoupling of the respiratory chain (Charton et al., 2004). Therefore, MTT assays were used to estimate the minimal concentration of oligomycin that could cause mitochondrial uncoupling in our cell lines, since reduction of the tetrazolium compound MTT is dependent on intact mitochondrial electron transport (Grazette et al., 2004). We observed an abrupt decrease in MTT reduction above an oligomycin concentration of 2.5–5 µg/ml, independent of the incubation time and the genetic background of all cell lines tested (Figure 6A; depicted are WM3734 as an example). These results are in line with oligomycin concentrations that were reported by others to specifically block oxidative phosphorylation (Hao et al., 2010). Thus, we considered oligomycin concentrations less than 2.5 µg/ml to work through the specific inhibition of the ATP-synthase and not through mitochondrial uncoupling.

We next asserted that low-dose oligomycin still leads to functional and significantly measurable effects, such as a decrease in ATP production or increase in lactate secretion in WM3734 cells (Figure 6B), and subsequently confirmed this for a panel of genetically different melanoma lines under normoxic and hypoxic conditions (Figure 6C). The detected changes in ATP and lactate were comparable to those measured by others for a number of different cell types (Hao et al., 2010). Interestingly, ATP-synthase inhibition was accompanied by a complete loss of endogenously expressed JARID1B protein after 72 hr of oligomycin treatment (Figure 6D). Also, the enrichment of JARID1B^{high} cells usually seen after hypoxic treatment was inhibited by low-dose oligomycin.

Due to the evolutionary link between nonproliferative and OXPHOS-dependent cell phenotypes (Berridge et al., 2010; Jose et al., 2011; Vander Heiden et al., 2009), we next asked if inhibition of mitochondrial ATP production also influences the cell cycle of melanoma cells. In fact, even very low doses of oligomycin (0.01 µg/ml) caused a measurable decrease in the percentage of cells in G1/0 phase and an increase in the percentage of cells in S- and G2/M-phase compared to vehicle controls. To optimize the readout, cells were serum-starved for 4 days and subsequently stimulated with FCS for 8 and 16 hr (Figure 6E). After 24 hr, cell cycle phases were again equal in oligomycin and vehicle control-treated cell groups (data not shown). Despite the increase in proliferative cell cycle phases, we found a relative decrease in overall cell numbers after oligomycin treatment compared to controls (Figure 6F). A likely explanation for this paradox is that simultaneously to (or after) the acceleration of the cell cycle, a considerable portion of the cells is undergoing cell death, as indicated by independently performed 7AAD staining and subsequent flow cytometric analysis (e.g., ~20% dead cells after 72 hr of 0.1 µg/ml oligomycin; Figure S4A). Short-term analysis of oligomycin's effect on total cell numbers showed that the cell population slightly expands at low doses (Figure 6F, left panel), whereas high doses starting from 5 µg/ml caused persisting or decreasing cell numbers, possibly due to highly toxic mitochondrial uncoupling. The full effect of the antitumor potential of low-dose oligomycin became visible in long-term colony formation assays. Here, a significant reduction in colony growth was seen after 3 weeks of treatment (Figure 6F, right panel), which is reminiscent of the results previously reported for JARID1B knockdown (Roesch et al., 2010). Short-term treatment of WM3734 cells with the ATP-synthase inhibitor

Bz-423 and the complex I inhibitors rotenone and phenformin confirmed these findings (Figures S4B–S4D). In conclusion, this suggests that pharmacological targeting of the mitochondrial respiratory chain can inhibit the JARID1B^{high} slow-cycling subpopulation and reveal long-term suppressive effects in melanoma cells.

Inhibition of the Mitochondrial Respiratory Chain Overcomes Intrinsic Multidrug Resistance of Melanoma

We asked if inhibition of the mitochondrial respiration could counteract the intrinsic multidrug resistance mediated by slow-cycling melanoma cells. Flow cytometric quantitation of J/EGFP levels in WM3734 cells (Figure 7A) and 1205LU cells (Figure S5A) revealed a significant blockade of the JARID1B^{high} subpopulation when cells were treated with the combination of cisplatin plus oligomycin. Similar results were seen for Bz-423, which also acts as an ATP-synthase inhibitor (Figure S5B). Even treatment with extremely low doses of oligomycin (0.001 µg/ml; Figure S5C) still blocked the enrichment of J/EGFP^{high} cells. At 0.001 µg/ml, single-agent oligomycin did not induce substantial cell death, as measured by 7AAD flow cytometry in WM3734 cells (Figure S4A); however, when combined with cisplatin, the overall number of dead cells strongly increased (Figure S5C). Immunoblots revealed a complete loss of endogenous JARID1B under oligomycin cotreatment, overcoming the cisplatin-induced enrichment of JARID1B protein after 24, 48, and 72 hr (Figure 7A). Cytotoxicity assays confirmed that the combination with oligomycin sensitizes melanoma cells to cisplatin treatment, but depending on the cell line used, the contribution of single-agent oligomycin to cell killing can vary (Figure 7B). MeWo cells, the melanoma cell line with the lowest oligomycin response in lactate secretion (Figure 6C), were not sensitized to cisplatin, indicating that the combination with oligomycin is not universally cytotoxic, but instead, responses match our mitochondrial activity-based hypothesis. The tumor suppressive potential of combinatorial ATP-synthase inhibition was further demonstrated in 3D collagen-embedded spheroids of 1205Lu cells, a model which more readily mimics the melanoma microenvironment. The combination of oligomycin plus vemurafenib more potently inhibited cell invasion into collagen than each drug alone (Figure 7C; p < 0.0003). Notably, treatment of WM3734 cells with a single pulse of low-dose oligomycin plus cisplatin over 72 hr substantially reduced long-term growth in soft agar and the number of 3D colonies remained at almost undetectable levels, even after 5 weeks of culture in drug-free medium (Figure 7D). This effect reached statistical significance with p < 0.02 when large colonies above a diameter of 10 µm were counted. Consistent with the observation that significantly larger colonies grew from cisplatin pretreated cells (that were enriched for the J/EGFP^{high} subpopulation; Figure 4C), these results indicate that (1) adding mitochondrial inhibitors to common anticancer treatment significantly diminishes the number of cells with high repopulation and invasion potential and (2) that even a relatively short-term treatment can yield a sustained antitumor effect.

Mitochondrial inhibition as a combinatorial strategy against cancer drug-induced enrichment of slow-cycling JARID1B^{high} melanoma cells was further confirmed for the complex I inhibitors rotenone and phenformin. Phenformin is used in the clinics

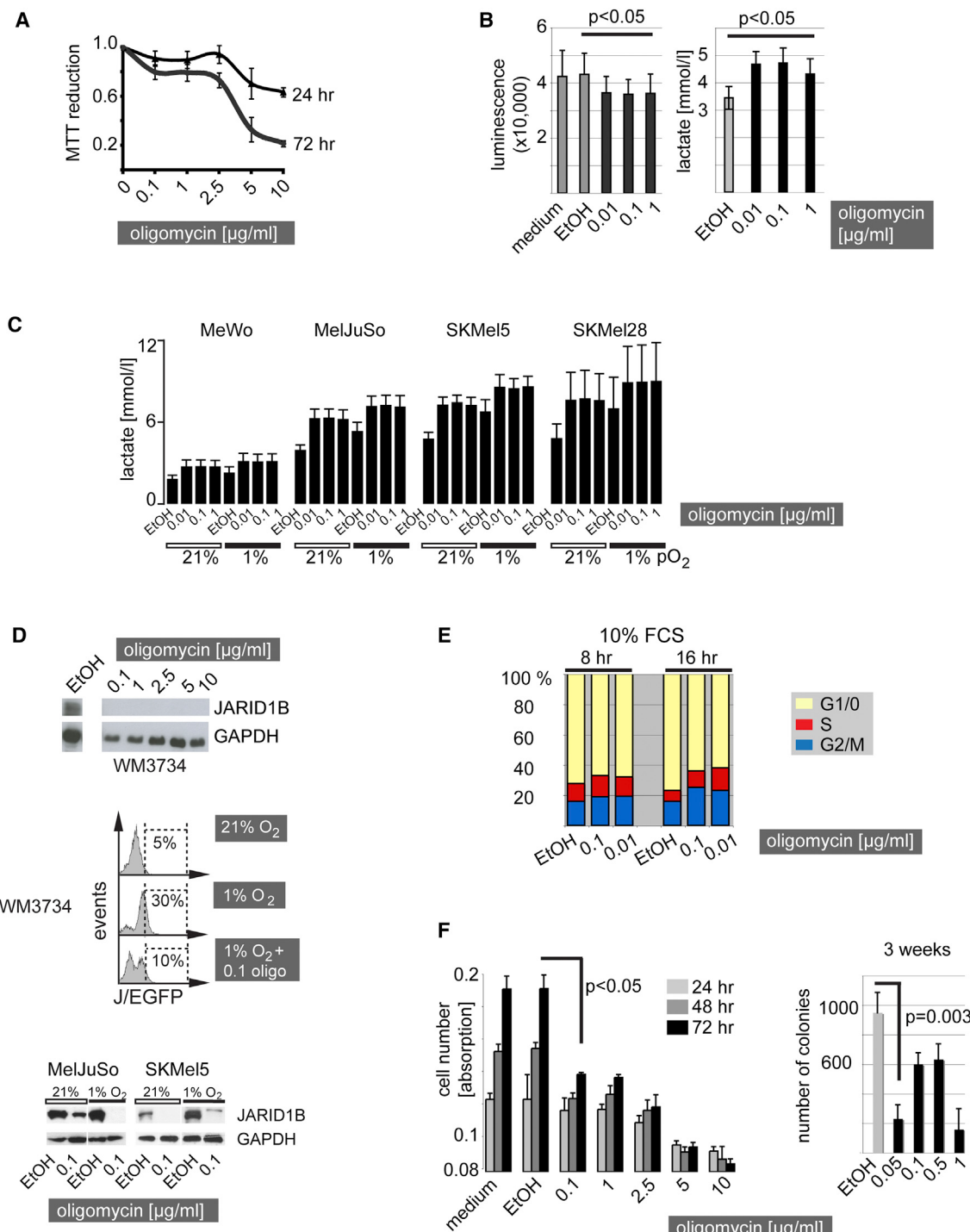


Figure 6. Inhibition of the Mitochondrial ATP Synthase Inhibits the JARID1B^{high} Subpopulation and Reveals Long-Term Melanoma Cell-Suppressive Effects

(A) MTT reduction curve of regularly cultured WM3734 melanoma cells after oligomycin treatment.

(B) Total cellular ATP levels were luminometrically determined in WM3734 cells after 24 hr of treatment with oligomycin at the indicated concentrations (left). Lactate production was measured in WM3734 cell culture supernatants after 24 hr of oligomycin. Ethanol (EtOH, diluted 1:1000) was used as vehicle control. Shown are means of three independently performed experiments.

(C) Lactate measurement in a panel of genetically diverse melanoma cell lines under normoxic versus hypoxic culture conditions after 24 hr of treatment.

(D) Immunoblot of JARID1B protein expression in WM3734 cells treated with oligomycin for 72 hr at the indicated concentrations (top). Frequency of J/EGFP^{high} WM3734 cells under 72 hr of hypoxia versus hypoxia plus oligomycin (oligo) treatment as determined by flow cytometry (middle). Immunoblots of endogenous JARID1B expression in MelJuSo and SKMel5 melanoma cells under hypoxia and hypoxia plus oligomycin treatment (bottom).

(legend continued on next page)

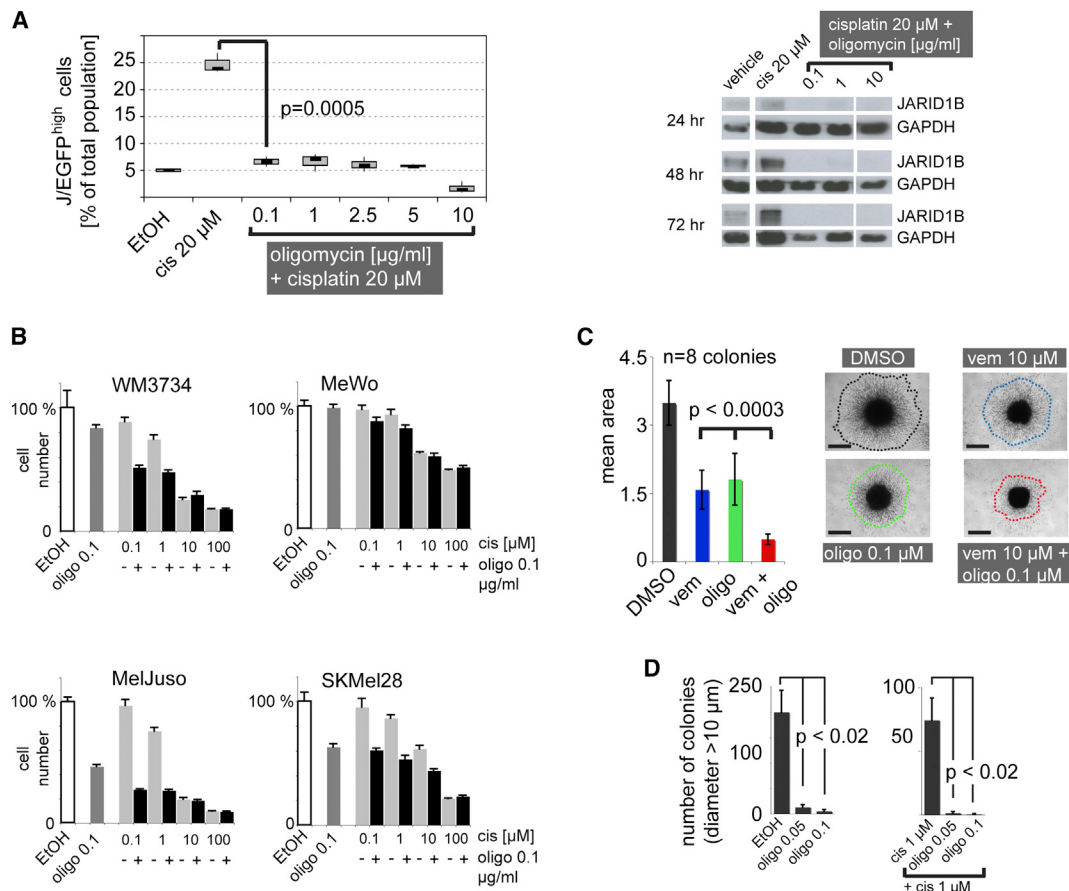


Figure 7. The Combination of Anticancer Agents plus Inhibition of the Mitochondrial ATP-Synthase Overcomes the Enrichment of the JARID1B^{high} Subpopulation In Vitro

(A) Relative percentage of the J/EGFP^{high} subpopulation under combinatorial treatment of WM3734 cells for 72 hr with cisplatin (*cis*) and oligomycin as determined by flow cytometry (left). Ethanol (EtOH) was used as vehicle control. Immunoblots of the endogenous JARID1B protein expression of WM3734 cells under cotreatment with oligomycin at the indicated time points (right).

(B) Cytotoxicity assays of melanoma cell lines after 72 hr of cotreatment with cisplatin (*cis*) and oligomycin (oligo).

(C) Three-dimensional growth/invasion/survival assay of 1205Lu cells treated with vemurafenib (vem) and oligomycin (oligo) for 96 hr. Colony sizes were quantified digitally based on the relative number of pixels. Scale bar represents 500 μ m.

(D) Soft agar colony-forming assay of WM3734 cells after 72 hr pulse treatment with oligomycin (left) and oligomycin plus cisplatin (right). Colonies were counted manually after 5 weeks of growth. Results shown from one of two independent experiments. Error bars represent SD.

See also Figure S5.

as an antidiabetic drug. Both compounds potently blocked the emergence of JARID1B^{high} cells during antimelanoma treatment (Figures 8A and S6A–S6D). Immunoblots and immunohistochemistry of phenformin-treated cells confirmed that complex I inhibition affects the endogenous JARID1B phenotype in vitro and in vivo (Figures S6C and S6D). Similar to the combinations of bortezomib or vemurafenib with JARID1B gene knockdown shown in Figure 3D, the mitochondrial inhibition by phenformin improved the tumor-suppressive potential of vemurafenib in xenotransplanted melanomas in vivo (Figures 8B and S6D). Sta-

tistical overall significance was shown by MANOVA ($p = 0.0263$). Significant differences between the combination and single treatments were seen after adjusting for multiple hypothesis testing (combination versus vemurafenib was $p = 0.022$, versus phenformin $p = 0.010$, and versus control $p = 0.010$). Altogether, these findings suggest that multiresistant, slow-cycling melanoma cells are susceptible to the inhibition of the mitochondrial respiratory chain and that the oxidative energy metabolism could be a prime target to overcome intrinsic drug resistance in melanoma.

(E) WM3734 cells were starved at 0% FCS and then released by 10% FCS for 8 and 16 hr. The bar graph shows one example of three independent experiments of propidium iodide-based cell cycle analysis. Dead cells (SubG1) were gated out.

(F) Short-term effects of increasing concentrations of oligomycin on total WM3734 cell numbers as determined by crystal violet assays (left). Long-term growth reduction as measured by 3D soft agar colony formation assays (bidaily treatment, right). Error bars represent SD.

See also Figure S4.

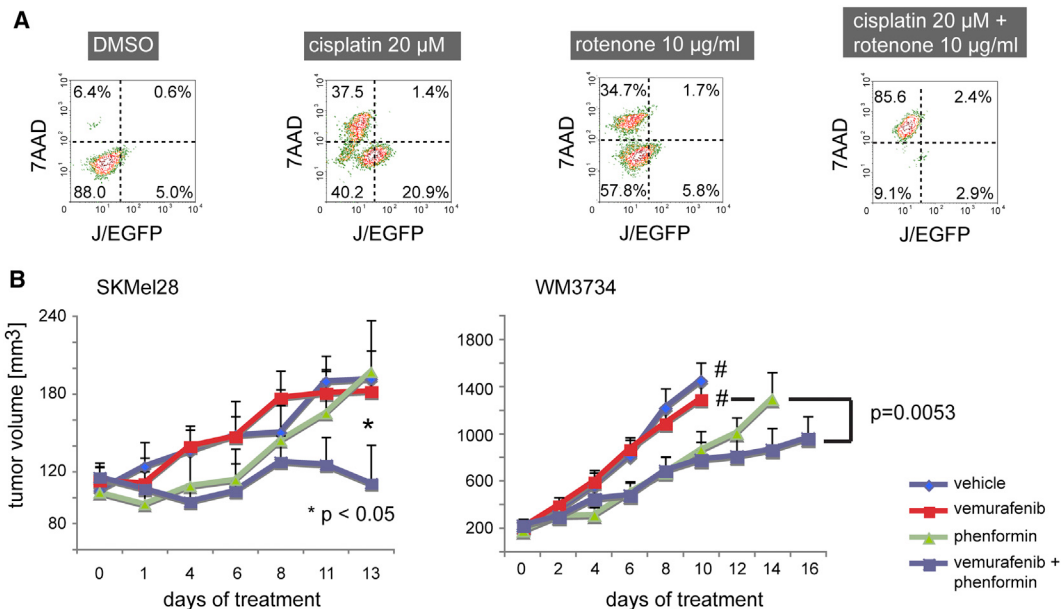


Figure 8. The Effect of Anticancer Agents Is Increased In Vitro and In Vivo by the Combination with Complex I Inhibitors

(A) Flow cytometric pattern of 7AAD and J/EGFP signals in cultured WM3734 cells after 72 hr of treatment with cisplatin and rotenone.

(B) SCID beige mice were xenotransplanted with 10^5 SKMel28 human melanoma cells (left, n = 7 per treatment group, n = 6 in vehicle group), NSG mice with 5×10^4 WM3734 cells (right, n = 8 per group). SKMel28 tumors were treated when an average volume of $\sim 120 \text{ mm}^3$ was reached, WM3734 tumors at an average volume of 200 mm^3 . Tumor volumes were assessed every other day. Groups marked with # were terminated earlier due to excessive tumor growth. Error bars represent SEM.

See also Figure S6.

DISCUSSION

Despite recent discoveries in the area of therapy resistance in melanoma, we do not fully know how therapeutic escape arises and if it is the result of an evolutionary process under treatment, from the selection of pre-existing resistant subpopulations, or a combination of both. Likely, even among functionally and genetically heterogeneous tumors, common mechanisms may exist that allow cells to survive in harsh conditions in general. Based on our experience with vemurafenib-resistant clones in vitro, we observed that functionally acquired resistance in cell lines that are initially vemurafenib-sensitive takes time to develop but eventually leads to reactivation of the MAPK and PI3K pathways (Villanueva et al., 2010). Intrinsic resistance conferred by the slow-cycling cell phenotype could represent an additional and universal protection mechanism that helps cells survive the very first contact with various cytotoxic agents and provides cells with added survival time to establish longer-lasting secondary resistance mechanisms. A major challenge for successful therapy is that these slow-cycling cells can be present at any stage of the disease and that this phenotype can be dynamically acquired by other melanoma cells, depending on the microenvironmental context, thus representing a “moving target” (Roesch et al., 2005, 2010).

Our findings indicate that the slow-cycling phenotype reflects a metabolic state that is characterized by high expression of mitochondrial bioenergetic enzymes relative to the rapidly proliferating tumor bulk population. Otto Warburg predicted that cancer cells generally rely on an increase in glucose uptake,

the enhancement of glycolysis and lactate production, along with the absence of oxidative respiration, despite the presence of sufficient oxygen concentrations (Warburg et al., 1924). He erroneously suggested defective mitochondria as a possible cause. However, it is becoming clear now that mitochondria in cancer cells are mostly intact and may play an important role in tumor growth (Caro et al., 2012; Weinberg et al., 2010). The cells’ decision to employ glycolysis or oxidative phosphorylation for their energy supply depends on multiple factors, including the cancer type and stage, the sequence of oncogenes activated, which can directly influence mitochondrial metabolism, the current microenvironmental context, and also the rate of cell proliferation (Berridge et al., 2010; Jose et al., 2011; Vander Heiden et al., 2009). Our results support the general hypothesis that slow-cycling cells rely more on oxidative phosphorylation, whereas rapidly growing cells are characterized by high glycolysis (Berridge et al., 2010; Jose et al., 2011; Vander Heiden et al., 2009). As previously shown by others, the blockage of glycolysis by bromopyruvate treatment is only efficient on rapidly growing cells and barely useful to decrease the growth rate of tumor cells with slow proliferation (Jose et al., 2011). This observation together with ours indicates that cell cycling and energy metabolism represent interwoven biologic processes that holistically contribute to the phenotype of tumor cell subpopulations. With regard to intrinsic drug susceptibility, we found that the JARID1B^{high} slow-cycling phenotype is not responding to exogenous cell cycle influences, such as serum starvation (data not shown). Since depletion of JARID1B does affect cell cycle phases, we would consider JARID1B expression to be a “driver”

of the slow-cycling phenotype rather than a “passenger.” Treatment with the multi-cyclin-dependent kinase (CDK) inhibitor dinaciclib resulted in massive cell death rather than in proliferation arrest and thus passively selected for JARID1B^{high} cells, as seen before for other anticancer agents (data not shown). We further suggest that consideration of single biologic features, such as cell cycling, without the metabolic contribution may not be sufficient to predict therapeutic response. For example, MeWo cells, which are known to have a high ability to metabolize glutamine in the (reversed) tricarboxylic acid (TCA) cycle as an alternative energy source (Scott et al., 2011), responded least to cytotoxic killing and mitochondrial inhibition, although having a rather high proliferation rate (and low endogenous JARID1B expression; data not shown).

We cannot exclude the possibility that our initial proteome profiling strategy may have missed additional important factors contributing to the biology of slow-cycling cells. Therefore, we analyzed common molecular players of melanoma tumorigenesis by immunoblotting of sorted J/EGFP^{high} versus J/EGFP^{low} cells. We found no difference in MAPK activation (measured by pMEK and pERK levels) nor in the expression of the apoptosis markers BCL-2, MCL-1, and BIM or the cell-cycle regulators CDK2, CDK4, and CDK9 (data not shown). Interestingly, we found an increase in pAKT in J/EGFP^{high} cells that correlates well with our previous finding that reactivation of PI3K signaling can overcome vemurafenib’s cytotoxicity in melanoma cells (Vilanueva et al., 2010). The relevance of this finding with regard to therapeutic strategies comprising combinatorial inhibition of PI3K in slow-cycling cells will be the subject of future studies. Considering the heterogeneity of melanoma, we are currently delineating additional molecular mechanisms underlying resistance of the JARID1B^{high} slow-cycling phenotype. However, non-JARID1B-related phenotypic resistance is likely to occur, and all potential resistance mechanisms could contribute to melanoma recurrence.

Our data confirm that slow-cycling melanoma cells of different genetic backgrounds are intrinsically resistant to various anti-cancer drugs and are characterized by the presence of several key enzymes of oxidative energy metabolism. Depletion of the JARID1B^{high} slow-cycling phenotype either by gene knockdown or by targeting of its bioenergetic metabolism sensitizes melanoma for a more pronounced and long-lasting therapeutic effect. Selective targeting of the slow-cycling subpopulation in combination with conventional tumor “debulking” strategies could help to eliminate a dramatically higher percentage of melanoma cells and significantly prolong the therapeutic response in patients with malignant melanoma.

EXPERIMENTAL PROCEDURES

Melanoma Cell Lines, Tissue, and Vector Constructs

Establishment and studying of noncommercial melanoma cell lines from human tumor samples was approved by the Internal Review Boards of the University of Pennsylvania School of Medicine and The Wistar Institute. Immunohistochemical staining of human melanoma samples was approved by the ethics committees of the University of Frankfurt and the Saarland University. Informed consents were obtained from all participating subjects. For details on cell culture techniques, see *Supplemental Experimental Procedures*. The consistency of cellular genotypes was confirmed by DNA fingerprinting at the Department of Human Genetics of The Saarland University Hospital. The lenti-

viral vector constructs for stable knockdown of JARID1B were purchased from Sigma. Details on lentiviral pL-U-JARID1B-prom-EGFP-Blast, pL-U-CMV-prom-EGFP-Blast, and transient transfection with pBIND-RBP2H1(JARID1B) were previously described (Roesch et al., 2008, 2010).

Detection of JARID1B and Flow Cytometry of J/EGFP Signals

For immunoblotting and immunostaining, rabbit polyclonal anti-JARID1B antibodies (Novus NB100-97821 and 22260002) were used, following established protocols (Roesch et al., 2010). Quantitative real time RT-PCR was performed on a StepOnePlus instrument (Applied Biosystems) using self-designed primers or primers from the Harvard primer bank as described earlier (Roesch et al., 2010). Flow cytometric detection of JARID1B promoter-driven EGFP signals was performed using a FACSCanto II (BD Biosciences) as described in the supplements. Dead cells were excluded by staining for 7AAD. Fluorescence-activated cell sorting was done on a Cytomation MoFlo (DakoCytomation) or a FACS Aria II (BD Biosciences) instrument.

Cell Proliferation and Three-Dimensional Growth/Invasion/Survival Assays

Cell proliferation was quantified by MTT and crystal violet assays according to standard protocols. Anchorage-independent colony formation was measured in 0.35% soft agar assays and quantified manually or digitally as described before using Image Pro Plus 7.0 (Roesch et al., 2010). Collagen-embedded, three-dimensional melanoma spheroids were prepared and treated with inhibitors at the designated concentrations for 72 hr, as previously described (Smalley et al., 2006). Following treatment, spheroids were imaged using a Nikon-300 inverted fluorescence microscope. To quantitate invasion into the matrix, borders were established around the invasive edge based on an ImageJ-defined cell density parameter, and the same parameters were applied to all images.

Measurement of ATP and Lactate

Total cellular ATP was measured using the ATP-based CellTiter-Glo kit (Promega) according to the manufacturer’s instructions. Each well on a 96 well plate was seeded with 2,000 cells, which were incubated with compounds at designated concentrations over varying time points (1, 2, 4, and 24 hr). Luminescence was measured on a Tecan M200 Infinite plate reader. Mitochondrial ATP levels were determined using the mitochondrial ATP sensor protein A_{TEAM} as reported (Imamura et al., 2009) and described in the *Supplemental Information*. For lactate measurement, 10⁵ cells were plated per well on a six well plate and treated with compounds over 6, 24, or 72 hr. Cell culture supernatant (500 µl) was collected and centrifuged to remove any cellular debris. Subsequently, an aliquot of 100 µl was analyzed using Roche’s automated Modular Analytics system.

In Vivo Melanoma Models

All animal experiments were performed in accordance with institutional and national guidelines and regulations. The protocols have been approved by the Wistar IACUC or the Saarland Veterinary Administration. NSG and severe combined immunodeficiency (SCID) beige mice were used for xenotransplantation. WM3734 or SKMel28 human melanoma cells were subcutaneously injected at a Matrigel/culture medium ratio of 1:1. Mice were treated with (1) bortezomib every other day (20 µg per intraperitoneal injection), (2) with vemurafenib every 12 hr (100 mg/kg per oral gavage), or (3) for combination studies with vemurafenib (15 mg/kg) plus phenformin (150 mg/kg; Appleyard et al., 2012) every 12 hr. Buffered saline or 0.1% Tween 80/0.5% methylcellulose served as vehicle controls. Treatment started at an average tumor volume of ~120–200 mm³. Tumor growth was measured every 2 or 3 days using a caliper. Tumor volumes were calculated according to the formula $V = W \times D \times H / [mm^3]$.

Statistics

MANOVA was used to evaluate differences between treatment groups; the change in the natural logarithm of volume over time was estimated for each animal from a linear regression, and mean slopes were compared using a t test. For the SKMel28 animal study, p values were adjusted according to Hochberg (1988). The two-sided Wilcoxon two-sample test was used when assumptions for the t test were violated (Figure 3A); otherwise, the Student’s

t test was used. Box plots show the sample minimum (lower whisker), the lower quartile (bottom of the box), the median (line inside the box), the upper quartile (top of the box), and the sample maximum (upper whisker). A p value of less than 0.05 was considered significant. As software tools, SAS version 9.2 using Proc GLM and Microsoft Excel were used.

SUPPLEMENTAL INFORMATION

Supplemental Information includes Supplemental Experimental Procedures, six figures, and one table and can be found with this article online at <http://dx.doi.org/10.1016/j.ccr.2013.05.003>.

ACKNOWLEDGMENTS

We thank K. Speicher and T. Beer (Wistar Proteomics Facility), J. Hayden and F. Keeney (Wistar Microscopy Facility), J.S. Faust (Wistar Flow Cytometry Facility), R. DelGiacco (Wistar Histology Facility), C. Junker and R. Kappl (Department of Biophysics, The Saarland University), and A. Liu (Department of Neurology, The Saarland University Hospital) for technical support and S. Kugler, H. Palm, A. Stark, A. Kerber, R. Koerner (Department of Dermatology, The Saarland University Hospital), and G. Rajan (Wistar Melanoma Research Center) for technical assistance. The animals were housed at Wistar's Animal Facility and the Institute for Clinical and Experimental Surgery, The Saarland University. Lactate measurement was done at the Department of Clinical Chemistry of The Saarland University Hospital. We also thank N. Demaurex, H. Imamura, and H. Noji for providing the A_{TEAM} probe, V. Belousov for Hyper, and B. Niemeyer for the JARID1B pCAGGS-IRES-RFP construct. The research was funded by NIH grants CA25874, CA047159, and CA10815, the Dr. Miriam and Sheldon G. Adelson Medical Research Foundation, and DFG grants SFB1027 project C4, SFB 894 (A1), R3577/2-1, and R3577/3-1.

Received: May 31, 2012

Revised: November 28, 2012

Accepted: May 1, 2013

Published: June 10, 2013

REFERENCES

- Appleyard, M.V., Murray, K.E., Coates, P.J., Wullschleger, S., Bray, S.E., Kernohan, N.M., Fleming, S., Alessi, D.R., and Thompson, A.M. (2012). Phenformin as prophylaxis and therapy in breast cancer xenografts. *Br. J. Cancer* **106**, 1117–1122.
- Berridge, M.V., Herst, P.M., and Tan, A.S. (2010). Metabolic flexibility and cell hierarchy in metastatic cancer. *Mitochondrion* **10**, 584–588.
- Blagosklonny, M.V. (2005). Why therapeutic response may not prolong the life of a cancer patient: selection for oncogenic resistance. *Cell Cycle* **4**, 1693–1698.
- Caro, P., Kishan, A.U., Norberg, E., Stanley, I.A., Chapuy, B., Ficarro, S.B., Polak, K., Tondera, D., Gounaris, J., Yin, H., et al. (2012). Metabolic signatures uncover distinct targets in molecular subsets of diffuse large B cell lymphoma. *Cancer Cell* **22**, 547–560.
- Charton, C., Ułaszewski, S., da Silva Vieira, M.R., Henoux, V., and Claisse, M.L. (2004). Effects of oligomycins on adenosine triphosphatase activity of mitochondria isolated from the yeasts *Saccharomyces cerevisiae* and *Schwanniomyces castellii*. *Biochem. Biophys. Res. Commun.* **318**, 67–72.
- Chen, K.G., Valencia, J.C., Gillet, J.P., Hearing, V.J., and Gottesman, M.M. (2009). Involvement of ABC transporters in melanogenesis and the development of multidrug resistance of melanoma. *Pigment Cell Melanoma Res.* **22**, 740–749.
- Chen, J., Li, Y., Yu, T.S., McKay, R.M., Burns, D.K., Kernie, S.G., and Parada, L.F. (2012). A restricted cell population propagates glioblastoma growth after chemotherapy. *Nature* **488**, 522–526.
- Christensen, J., Agger, K., Cloos, P.A., Pasini, D., Rose, S., Sennels, L., Rappaport, J., Hansen, K.H., Salcini, A.E., and Helin, K. (2007). RBP2 belongs to a family of demethylases, specific for tri-and dimethylated lysine 4 on histone 3. *Cell* **128**, 1063–1076.
- Dey, B.K., Stalker, L., Schnurch, A., Bhatia, M., Taylor-Papadimitriou, J., and Wynder, C. (2008). The histone demethylase KDM5b/JARID1b plays a role in cell fate decisions by blocking terminal differentiation. *Mol. Cell. Biol.* **28**, 5312–5327.
- Grazette, L.P., Boecker, W., Matsui, T., Semigran, M., Force, T.L., Hajjar, R.J., and Rosenzweig, A. (2004). Inhibition of ErbB2 causes mitochondrial dysfunction in cardiomyocytes: implications for herceptin-induced cardiomyopathy. *J. Am. Coll. Cardiol.* **44**, 2231–2238.
- Gupta, P.B., Onder, T.T., Jiang, G., Tao, K., Kuperwasser, C., Weinberg, R.A., and Lander, E.S. (2009). Identification of selective inhibitors of cancer stem cells by high-throughput screening. *Cell* **138**, 645–659.
- Hao, W., Chang, C.P., Tsao, C.C., and Xu, J. (2010). Oligomycin-induced bioenergetic adaptation in cancer cells with heterogeneous bioenergetic organization. *J. Biol. Chem.* **285**, 12647–12654.
- Hochberg, Y. (1988). A sharper Bonferroni procedure for multiple tests of significance. *Biometrika* **75**, 800–802.
- Imamura, H., Nhat, K.P., Togawa, H., Saito, K., Iino, R., Kato-Yamada, Y., Nagai, T., and Noji, H. (2009). Visualization of ATP levels inside single living cells with fluorescence resonance energy transfer-based genetically encoded indicators. *Proc. Natl. Acad. Sci. USA* **106**, 15651–15656.
- Johannessen, C.M., Boehm, J.S., Kim, S.Y., Thomas, S.R., Wardwell, L., Johnson, L.A., Emery, C.M., Stransky, N., Cogdill, A.P., Barretina, J., et al. (2010). COT drives resistance to RAF inhibition through MAP kinase pathway reactivation. *Nature* **468**, 968–972.
- Jose, C., Bellance, N., and Rossignol, R. (2011). Choosing between glycolysis and oxidative phosphorylation: a tumor's dilemma? *Biochim. Biophys. Acta* **1807**, 552–561.
- Nazarian, R., Shi, H., Wang, Q., Kong, X., Koya, R.C., Lee, H., Chen, Z., Lee, M.K., Attar, N., Sazegar, H., et al. (2010). Melanomas acquire resistance to B-RAF(V600E) inhibition by RTK or N-RAS upregulation. *Nature* **468**, 973–977.
- Poulkakos, P.I., Persaud, Y., Janakiraman, M., Kong, X., Ng, C., Moriceau, G., Shi, H., Atefi, M., Titz, B., Gabay, M.T., et al. (2011). RAF inhibitor resistance is mediated by dimerization of aberrantly spliced BRAF(V600E). *Nature* **480**, 387–390.
- Roesch, A., Becker, B., Meyer, S., Wild, P., Hafner, C., Landthaler, M., and Vogt, T. (2005). Retinoblastoma-binding protein 2-homolog 1: a retinoblastoma-binding protein downregulated in malignant melanomas. *Mod. Pathol.* **18**, 1249–1257.
- Roesch, A., Becker, B., Schneider-Brachert, W., Hagen, I., Landthaler, M., and Vogt, T. (2006). Re-expression of the retinoblastoma-binding protein 2-homolog 1 reveals tumor-suppressive functions in highly metastatic melanoma cells. *J. Invest. Dermatol.* **126**, 1850–1859.
- Roesch, A., Mueller, A.M., Stempfli, T., Moehle, C., Landthaler, M., and Vogt, T. (2008). RBP2-H1/JARID1B is a transcriptional regulator with a tumor suppressive potential in melanoma cells. *Int. J. Cancer* **122**, 1047–1057.
- Roesch, A., Fukunaga-Kalabis, M., Schmidt, E.C., Zabierowski, S.E., Brafford, P.A., Vultur, A., Basu, D., Gimotty, P., Vogt, T., and Herlyn, M. (2010). A temporarily distinct subpopulation of slow-cycling melanoma cells is required for continuous tumor growth. *Cell* **141**, 583–594.
- Scott, D.A., Richardson, A.D., Filipp, F.V., Knutzen, C.A., Chiang, G.G., Ronai, Z.A., Osterman, A.L., and Smith, J.W. (2011). Comparative metabolic flux profiling of melanoma cell lines: beyond the Warburg effect. *J. Biol. Chem.* **286**, 42626–42634.
- Sharma, S.V., Lee, D.Y., Li, B., Quinlan, M.P., Takahashi, F., Maheswaran, S., McDermott, U., Azizian, N., Zou, L., Fischbach, M.A., et al. (2010). A chromatin-mediated reversible drug-tolerant state in cancer cell subpopulations. *Cell* **141**, 69–80.
- Smalley, K.S., Haass, N.K., Brafford, P.A., Lioni, M., Flaherty, K.T., and Herlyn, M. (2006). Multiple signaling pathways must be targeted to overcome drug resistance in cell lines derived from melanoma metastases. *Mol. Cancer Ther.* **5**, 1136–1144.
- Sosman, J.A., Kim, K.B., Schuchter, L., Gonzalez, R., Pavlick, A.C., Weber, J.S., McArthur, G.A., Hutson, T.E., Moschos, S.J., Flaherty, K.T., et al.

- (2012). Survival in BRAF V600-mutant advanced melanoma treated with vemurafenib. *N. Engl. J. Med.* **366**, 707–714.
- Vander Heiden, M.G., Cantley, L.C., and Thompson, C.B. (2009). Understanding the Warburg effect: the metabolic requirements of cell proliferation. *Science* **324**, 1029–1033.
- Villanueva, J., Vultur, A., Lee, J.T., Somasundaram, R., Fukunaga-Kalabis, M., Cipolla, A.K., Wubbenhorst, B., Xu, X., Gimotty, P.A., Kee, D., et al. (2010). Acquired resistance to BRAF inhibitors mediated by a RAF kinase switch in melanoma can be overcome by cotargeting MEK and IGF-1R/PI3K. *Cancer Cell* **18**, 683–695.
- Wagle, N., Emery, C., Berger, M.F., Davis, M.J., Sawyer, A., Pochanard, P., Kehoe, S.M., Johannessen, C.M., Macconail, L.E., Hahn, W.C., et al. (2011). Dissecting therapeutic resistance to RAF inhibition in melanoma by tumor genomic profiling. *J. Clin. Oncol.* **29**, 3085–3096.
- Warburg, O., Posener, K., and Negelein, E. (1924). Ueber den stoffwechsel der tumoren. *Biochem. Z.* **152**, 319–344.
- Weinberg, F., Hamanaka, R., Wheaton, W.W., Weinberg, S., Joseph, J., Lopez, M., Kalyanaraman, B., Mutlu, G.M., Budinger, G.R., and Chandel, N.S. (2010). Mitochondrial metabolism and ROS generation are essential for Kras-mediated tumorigenicity. *Proc. Natl. Acad. Sci. USA* **107**, 8788–8793.
- White, R.M., Cech, J., Ratanasirinawoot, S., Lin, C.Y., Rahl, P.B., Burke, C.J., Langdon, E., Tomlinson, M.L., Mosher, J., Kaufman, C., et al. (2011). DHODH modulates transcriptional elongation in the neural crest and melanoma. *Nature* **471**, 518–522.
- Xia, X., Lemieux, M.E., Li, W., Carroll, J.S., Brown, M., Liu, X.S., and Kung, A.L. (2009). Integrative analysis of HIF binding and transactivation reveals its role in maintaining histone methylation homeostasis. *Proc. Natl. Acad. Sci. USA* **106**, 4260–4265.
- Yamane, K., Tateishi, K., Klose, R.J., Fang, J., Fabrizio, L.A., Erdjument-Bromage, H., Taylor-Papadimitriou, J., Tempst, P., and Zhang, Y. (2007). PLU-1 is an H3K4 demethylase involved in transcriptional repression and breast cancer cell proliferation. *Mol. Cell* **25**, 801–812.